colloids and interfaces

MDPI

Article

Ethanolic Cashew Leaf Extract Encapsulated in Tripolyphosphate–Chitosan Complexes: Characterization, Antimicrobial, and Antioxidant Activities

Pitima Sinlapapanya [1], Jirayu Buatong [1], Suriya Palamae [1], Rasool Abdul Nazeer [2], Bin Zhang [3], Thummanoon Prodpran [4] and Soottawat Benjakul [1,5,*]

1 International Center of Excellence in Seafood Science and Innovation, Faculty of Agro-Industry, Prince of Songkla University, Hat Yai, Songkhla 90110, Thailand; pitimasinlapapanya@gmail.com (P.S.); jirayu.b@psu.ac.th (J.B.); suriya.pal@psu.ac.th (S.P.)
2 Biopharmaceuticals Lab, Department of Biotechnology, School of Bioengineering, SRM Institute of Science and Technology, Kattankulathur 603203, Tamilnadu, India; nazeerr@srmist.edu.in
3 Key Laboratory of Health Risk Factors for Seafood of Zhejiang Province, College of Food Science and Pharmacy, Zhejiang Ocean University, Zhoushan 316022, China; zhangbin_ouc@163.com
4 Department of Material Product Technology, Faculty of Agro-Industry, Prince of Songkla University, Hat Yai, Songkhla 90110, Thailand; thummanoon.p@psu.ac.th
5 Department of Food and Nutrition at Kyung Hee University, Seoul 02447, Republic of Korea
* Correspondence: soottawat.b@psu.ac.th

Abstract: Ethanolic cashew leaf extract (ECL-E) is rich in phenolic compounds and shows remarkable antioxidative and antimicrobial activities. Encapsulation could stabilize ECL-E as the core. Tripolyphosphate (TPP)–chitosan (CS) nanoparticles were used to load ECL-E, and the resulting nanoparticles were characterized. The nanoparticles loaded with ECL-E at different levels showed differences in encapsulation efficiency (47.62–89.47%), mean particle diameters (47.30–314.60 nm), positive zeta potentials (40.37–44.24 mV), and polydispersity index values (0.20–0.56). According to scanning electron micrographs, the nanoparticles had a spherical or ellipsoidal shape, and a slight agglomeration was observed. The appropriate ratio of CS/ECL-E was 1:3, in which an EE of 89.47%, a particle size of 256.05 ± 7.70 nm, a zeta potential of 40.37 ± 0.66 mV, and a PDI of 0.22 ± 0.05 were obtained. The nanoparticles also exhibited high antioxidant activities, as assayed by DPPH and ABTS radical scavenging activities, ferric reducing ability power (FRAP), and oxygen radical absorbance capacity (ORAC). Low minimum inhibitory concentration and minimum bactericidal concentration were observed against *Pseudomonas aeruginosa* (9.38, 75.00 mg/mL) and *Shewanella putrefaciens* (4.69, 75.00 mg/mL). In addition, ECL-E loaded in nanoparticles could maintain its bioactivities under various light intensities (1000–4000 Lux) for 48 h. Some interactions among TPP, CS, and ECL-E took place, as confirmed by FTIR analysis. These nanoparticles had the increased storage stability and could be used for inactivating spoilage bacteria and retarding lipid oxidation in foods.

Keywords: cashew leaf extract; encapsulation; chitosan; antimicrobial; antioxidant; nanoparticle

Citation: Sinlapapanya, P.; Buatong, J.; Palamae, S.; Nazeer, R.A.; Zhang, B.; Prodpran, T.; Benjakul, S. Ethanolic Cashew Leaf Extract Encapsulated in Tripolyphosphate–Chitosan Complexes: Characterization, Antimicrobial, and Antioxidant Activities. *Colloids Interfaces* **2024**, *8*, 52. https://doi.org/10.3390/colloids8050052

Academic Editors: Reinhard Miller, Eleni P. Kalogianni and Julia Maldonado-Valderrama

Received: 15 August 2024
Revised: 6 September 2024
Accepted: 8 September 2024
Published: 10 September 2024

1. Introduction

Phenolic compounds are phytochemicals abundant in several plants, especially in cashew leaf extracts, that exhibit a wide range of biological activities [1,2]. Cashew leaf extract shows antioxidant and antimicrobial activities and can be used as a natural safe food additive [2,3]. However, some polyphenols are unstable and lose their bioavailability, which can be overcome through encapsulation [4,5].

Some bioactive substances and nutraceuticals need protection from external factors such as light, pH, temperature, oxygen, and enzymes. It is practicable to use micro- or nano-encapsulation to protect these substances [6]. Encapsulation in the form of microcapsules is an efficient method for safeguarding bioactive substances [7]. Encapsulated nutraceuticals

or bioactive compounds can be added to food matrices to create functional meals that are highly absorbed by the digestive system [8]. Bioactive compounds are loaded inside microcapsules during the encapsulation process, and they are then released at a specific time [9]. To encapsulate bioactive compounds and nutraceuticals, nano-encapsulation has drawn attention to creating stable nutrients for enriched foods [10]. Biodegradable polymers such as polylactic acid (PLA), poly(lactic-co-glycolic acid) (PLGA), and poly(glycerol adipate) (PGA) have been used to encapsulate bioactive compounds. However, there are still limitations related to low loading efficiency. Some of the produced compounds have side effects (toxicity), and these polymers have complicated synthesis steps [11]. Since several polysaccharides are highly modifiable, soluble, and capable of binding via their functional groups, they are appropriate for the encapsulation process as wall materials [7,10].

Because of its low toxicity, high biodegradability, and antibacterial qualities, chitosan, a linear polysaccharide produced by partially deacetylating chitin, has attracted special attention for a wide range of applications [12–15]. Furthermore, because its chain contains several functional groups, chitosan is easily modifiable to achieve appropriate physicochemical properties [12]. Chitosan is a widely used biocompatible polysaccharide for the development of pharmaceutical formulations such as gels, films, tissue engineering scaffolds, and nanoparticles. It also has antimicrobial properties [16].

The cationic character of chitosan is modified by a polyanion, like sodium tripolyphosphate (TPP), which causes ionotropic gelation, and the subsequent production of nanoparticles is achieved [17,18]. Bioactive substances have been encapsulated in chitosan nanoparticles and employed as delivery nanocarriers [19,20]. It has been demonstrated that chitosan nanoparticles have antibacterial properties, thermal stability, antioxidative activity, aqueous medium solubility, and increased release of bioactive chemicals [21,22]. As such, TPP-CS nanoparticles have potential applications as nanocarriers in food.

Cashew is an abundant plant in tropical areas, especially in the southern part of Thailand. Its nut has a high price and has become popular for consumers. As a consequence, the leaves are also available for the extraction of active compounds. Recently, cashew leaf extract has been reported to contain a wide range of polyphenolic compounds such as amentoflavone, quercetin, kaempferol, and catechin [2]. In addition, according to the previous report by Sinlapapanya et al. [3], it was found that phenolic compounds easily lose their activities when stored because of environmental factors such as light and heat. To maintain the bioactivities of the extract, coacervation could be a promising means to stabilize an extract exposed to the environment. The aim of the present study was to encapsulate ECL-E in TPP-CS nanoparticles. Nanoparticles were then characterized, and the antioxidant and antimicrobial activities of ECL-E loaded in nanoparticles were determined.

2. Materials and Methods

2.1. Chemicals

Ethanol was supplied by RCI Labscan Limited (Bangkok, Thailand). Chitosan (low molecular weight, 50–190 kDa) and sodium tripolyphosphate (TPP) were acquired from Sigma Aldrich, Inc. (St. Louis, MO, USA). Mueller–Hinton broth (MHB) and tryptic soy broth were obtained from Himedia (Mumbai, India).

2.2. Preparation of Ethanolic Cashew Leaf Extract (ECL-E) and the Encapsulation Process

2.2.1. Preparation of ECL-E

Dried cashew (*Anacardium occidentale* L.) leaves were powderized before extraction using 80% ethanol following the method explained by Sinlapapanya et al. [2]. Leaf powder (10 g) was mixed with 80% ethanol (200 mL) before ultrasonication at 70% amplitude for 40 min under pulsed mode (5s:5s) (Sonics, Model VC750, Sonica & Materials, Inc., Newtown, CT, USA). The temperature of the mixture during extraction was maintained below 35 °C. After that, the supernatant was collected and centrifuged (5000× *g*, 30 min, 4 °C) (Beckman Coulter, Avanti J-E Centrifuge, Fullerton, CA, USA). An Eyela rotary

evaporator (Tokyo Rikakikai, Co. Ltd., Tokyo, Japan) was employed to remove ethanol, and nitrogen flushing was applied to eliminate the remaining ethanol.

2.2.2. Dechlorophyllization of ECL-E

Chlorophylls in ECL-E were eliminated by the sedimentation process, as explained by Sinlapapanya et al. [3]. The extract and distilled water were mixed at 1:1 (v/v) ratio and properly mixed. After being chilled for 24 h, centrifugation (10,000× g, 30 min) was performed at 4 °C. The supernatant was freeze-dried and the final powder, known as "ethanolic cashew leaf extract" or "ECL-E", was packed in a zip-lock bag and kept at −20 °C.

2.2.3. TPP–Chitosan (TPP-CS) Encapsulation Process

Encapsulation via TPP-CS complexation was performed [7]. CS powder was dissolved in acetic acid solution (1% v/v) to gain the concentration of 1% (w/v). The mixture was stirred overnight, and centrifugation (9000× g, 10 min, 4 °C) was employed to remove the debris. ECL-E was mixed with CS solution (20 mL) to obtain varying CS/ECL-E ratios (1:1; 1:2; and 1:3) with the aid of homogenizer (IKA Labortechnik homogenizer, Selangor, Malaysia) at 13,000 rpm (Table 1). After pH adjustment to 4.2 with 2 M NaOH solution, TPP solution (0.4% w/v, 8 mL) was added dropwise with rigorous stirring to induce ionic gelation. Centrifugation (9000× g, 30 min, 4 °C) was used to separate TPP-CS gels from non-gelling substances, and the gels were dispersed in 100 mL of DI water containing 1% (w/v) trehalose. Then, the nanoparticles were prepared by dissociation of the flocculated pellet by ultrasonication (70% amplitude, 10 min) in pulse mode (5s:5s). TPP-CS complexes and TPP-CS complexes loaded with ECL-E were frozen (−40 °C) and lyophilized at −50 °C for 72 h by a freeze dryer (CoolSafe 55, ScanLaf A/S, Lynge, Denmark). Nanoparticles with CS/ECL-E ratios of 1:1, 1:2, and 1:3 were named as ECL-E-N-E1, ECL-E-N-E2, and ECL-E-N-E3, respectively. The nanoparticles were then analyzed.

Table 1. Encapsulation condition of ECL-E by the TPP-CS process.

Treatment	Ratio	EE (%)	PS (nm)	ZP (mV)	PDI	Color		
						L*	a*	b*
ECL-E	-	-	-	-	-	59.34 ± 0.07 ^{e}	1.33 ± 0.03 ^{a}	10.16 ± 0.04 ^{a}
TPP-CS	CS	43.01 ± 8.89 ^{b}	47.30 ± 4.60 ^{d}	43.96 ± 0.96 ^{a}	0.56 ± 0.06 ^{a}	63.02 ± 0.36 ^{d}	−0.54 ± 0.06 ^{d}	−0.65 ± 0.01 ^{d}
ECL-E-N-E1	CS(1):ECL-E(1)	47.62 ± 5.71 ^{b}	314.60 ± 20.65 ^{a}	44.24 ± 0.92 ^{a}	0.30 ± 0.03 ^{b}	64.71 ± 0.03 ^{c}	0.73 ± 0.05 ^{c}	10.07 ± 0.01 ^{b}
ECL-E-N-E2	CS(1):ECL-E(2)	86.72 ± 2.28 ^{a}	273.60 ± 3.70 ^{b}	41.13 ± 1.01 ^{b}	0.20 ± 0.02 ^{c}	66.91 ± 0.03 ^{b}	1.26 ± 0.02 ^{b}	9.73 ± 0.09 ^{c}
ECL-E-N-E3	CS(1):ECL-E(3)	89.47 ± 1.78 ^{a}	256.05 ± 7.70 ^{c}	40.37 ± 0.66 ^{b}	0.22 ± 0.05 ^{c}	69.55 ± 0.04 ^{a}	1.22 ± 0.05 ^{b}	10.10 ± 0.01 ^{a}

CS: chitosan, TPP: sodium tripolyphosphate, ECL-E: ethanolic cashew leaf extract, EE: encapsulation efficiency, PS: particle size, ZP: zeta potential, PDI: polydispersity index. Different lowercase superscripts within the same column indicate significant differences ($p < 0.05$). * Mean value ($n = 3$).

2.3. Analyses

2.3.1. Encapsulation Efficiency (EE)

The suspension of ECL-E-N was stirred gently for 30 min and centrifuged at 10,000× g for 15 min and 4 °C. The initial TPC of the dissolved ECL-E-N (M2) was noted.

$$\text{EE (\%)} = [1 - (\text{M1}/\text{M2})] \times 100$$

where M1 is the TPC outside the dialysis bag (in 200 mL of dialysis water) and M2 is the total TPC loaded.

2.3.2. Particle Size (PS), Polydispersity Index (PDI) and Zeta Potential Measurement

The dynamic light scattering technique was used to determine the PS, PDI, and zeta potential of different samples by the ZetaPlus zeta potential analyzer (Brookhaven Instruments Corporation, Holtsville, NY, USA) according to Tagrida et al. [23]. Ten milliliters of each sample suspension (10 mg/mL) was appropriately diluted in DI water and measured at 25 °C with a medium refractive index of 1.330. The particle size and PDI were determined at an angle of 90 °C.

2.3.3. Color

A colorimeter (ColorFlex, Hunter Lab Reston, VA, USA) was employed to examine the lightness (L*), redness/greenness (a*), and yellowness/blueness (b*) of different nanoparticles.

2.3.4. In Vitro Releasing Efficiency (RE)

A dialysis bag (2.5 × 10 cm, MW cut-off: 3500 Da) was used to examine the in vitro RE of different ECL-E-Ns compared with ECL-E [24]. One mL of 1% ECL-E (control) and various ECL-E-Ns (1 mg/mL, 100 mg/mL) were transferred into each dialysis bag, and the bags were clamped before dialysis in 100 mL of DI water by continuous stirring (100 rpm) for 72 h at 4 °C. Three milliliters of dialysis water were taken every 12 h up to 72 h for TPC analysis. RE was determined using the equation shown below.

$$\text{RE (\%)} = [1 - (\text{TPC}_{\text{release}}/\text{TPC}_{\text{total}})] \times 100$$

where RE denotes the release efficiency (%), $\text{TPC}_{\text{release}}$ (mg/mL) represents the TPC released after being dialyzed at the designated time (every 12 h), and $\text{TPC}_{\text{total}}$ (mg/mL) is the total TPC in ECL-E-Ns, obtained from the known amount of TPC in ECL-E used for preparation of nanoparticles.

For TPC determination, the Folin–Ciocalteu's reagent (FCR) method was adopted as described by Benjakul et al. [25]. TPC was expressed as mg gallic acid equivalent (GAE)/g dry solid.

2.3.5. Antioxidant Activities

ECL-E-Ns with different loading conditions (CS/ECL-E ratios) were tested for antioxidant activities in comparison with ECL-E (unencapsulated) [3].

ABTS Radical Scavenging Activity

A sample (150 µL) was mixed with ABTS solution (2850 µL) and incubated for 1 h at room temperature in the dark. Absorbance 734 nm was read. Blank was prepared using distilled water instead of a sample.

DPPH Radical Scavenging Activity

A sample (0.3 mL) was mixed with 2.7 mL of 0.15 mM DPPH in methanol, shaken, and incubated for 60 min at 25 °C in the dark. DPPH reduction was monitored by the decrease in OD at 517 nm.

Ferric Reducing Ability Power

A sample solution (150 µL) was mixed with 2.85 mL of working FRAP reagent, and the mixture was incubated in the dark at room temperature for 30 min. The absorbance at 593 nm was read.

Metal Chelating Activity

A sample (1 mL) was mixed with distilled water (3.7 mL). Subsequently, 2 mM $FeCl_2$ (0.1 mL) and 5 mM ferrozine (0.2 mL) were added. The absorbance at 562 nm was read after 20 min. For the control, 1 mL of distilled water was used to replace the extract.

Oxygen Radical Absorbance Capacity

The oxygen radical absorbance capacity (ORAC) assay was performed according to Sae-Leaw et al. [26].

Antioxidant activities were expressed as µmol Trolox equivalents (TE)/g dry solid, except metal chelating activity, which was reported as µmol EDTA equivalent (EE)/g dry solid.

The nanoparticle with the optimal CS/ECL-E ratio and the highest antioxidant activity was chosen for further analysis.

2.3.6. Antimicrobial Activity

Pseudomonas aeruginosa ATCC 27853, obtained from The American Type Culture Collection, and *Shewanella putrefaciens* JCM 20190, from the Japan Collection of Microorganisms, were used. Both bacteria are major spoilage bacteria commonly found in seafood. All bacteria were checked for purity before being used each time by re-streaking from the stock on TSA agar and selecting only a single colony for enrichment.

Minimum Inhibitory Concentration (MIC) and Minimum Bactericidal Concentration (MBC)

A Mueller–Hinton broth microdilution was adopted to evaluate the MIC and MBC of the ECL-E-Ns in a 96-well microplate [2]. The ECL-E-Ns were dissolved in DI water, and shaken vigorously, followed by filtration using a syringe. The filtrate from ECL-E-N (100 µL) was poured into a sterile 96-well plate at various concentrations (0.59–300 mg/mL). Bacterial inoculum (100 µL) in TSB medium with a concentration of 1×10^6 CFU/mL was added. A bacterial suspension with no extracts was employed as a positive control, whereas only extracts in the absence of bacterial suspension was used as a negative control [27]. The 96-well microplates were incubated at 37 °C for 15 h, and then 10 µL of rezasurin solution (0.18% *w*/*v*) was added to each well. The plate was incubated at 37 °C for 2–3 h. The MIC is the lowest concentration (bacteriostatic) of the extract at which there is no color change (blue color) detected. To validate the survival of bacteria, a suspension (10 µL) was taken from each well and spread on TSA agar before being incubated at 37 °C for 24 h. The MIC was the lowest concentration that inhibited the growth of bacteria, whereas the MBC was the lowest concentration of the agent that killed 99.9% of the bacteria or no growth was noted (bactericidal) [28].

2.3.7. Fourier Transform Infrared (FTIR) Spectroscopy

FTIR spectra of the free ECL-E fraction, empty nanoparticles, and ECL-E-loaded nanoparticles (ECL-E-Ns) were determined using an FTIR spectrometer (model Equinox 55, Bruker, Ettlingen, Germany) at a wavenumber between 4000 and 400 cm^{-1}. OPUS software (version 8.5 Bruker Optik GmbH 2020, Bruker, Ettlingen, Germany) was used for analysis.

2.3.8. Scanning Electron Microscopic (SEM) Images of ECL-E-Ns

The selected ECL-E-N samples were visualized using a scanning electron microscope (SEM, FEI Quanta 400-ESEM FEG, Hillsboro, OR, USA). Images were recorded as per the method explained by Sinlapapanya et al. [2].

2.4. Light Stability

The stability of the ECL-E-Ns toward light exposure under varying conditions was tested [3]. An ECL-E-N (10 mL, 50 mg/mL) was placed in a screw-cap test tube. After being exposed to light at varying intensities (1000, 2000, and 4000 lux), samples were taken every day for a total of 6 days for analyses of TPC, ABTS, DPPH, and radical scavenging activities as well as FRAP.

2.5. Statistical Analysis

The experiment was run in triplicate. The SPSS software program (SPSS 22.0 for Windows, SPSS Inc., Chicago, IL, USA) was used to perform an analysis of variance (ANOVA) and Duncan's multiple range test (DMRT) for mean comparisons.

3. Results and Discussion

3.1. Characteristics of ECL-E-Ns Prepared Using CS/ECL-E at Various Ratios by TPP-CS Complexation Methods

3.1.1. Encapsulation Efficiency (EE)

EE indicates the percentage of ECL-E present in nanoparticles. Depending on the CS/ECL-E ratio utilized, the EE of nanoparticles loaded with ECL-E varied from 43.01% to 89.47% (Table 1), suggesting that ECL-E was entrapped in nanoparticles to varied degrees.

CS/ECL-E ratios of 1:2 and 1:3 yielded the highest EE. There was a significant increase in EE ($p < 0.05$) when the CS/ECL-E ratio exceeded 1:1, which might have been caused by more ECL-E being entrapped in nanoparticles. When TPP was added, the positive charge of chitosan could be neutralized by the negative charge of the phosphate, forming a gel that could trap the ECL-E as its core.

EE can be higher with a high volume of extract because of several factors such as (a) increased cross-linking: a higher volume of extract may provide more active compounds that interact with chitosan, leading to better cross-linking with TPP, which stabilizes the nanoparticles and enhances encapsulation [29,30]; (b) higher availability of the encapsulating material: more extract means more material available to be encapsulated, increasing the likelihood of forming more complete nanoparticles with higher payloads [31]; and (c) enhanced viscosity: a greater volume of extract can increase the solution's viscosity, which may slow down particle aggregation and enhance encapsulation by allowing better dispersion of active compounds [32]. These combined phenomena likely contributed to higher EE when using a larger volume of extract in the TPP-CS encapsulation process.

3.1.2. Particle Size (PS), Zeta Potential (ZP), and Polydispersity Index (PDI) of ECL-E-Ns

The PS of different nanoparticles varied with different ratios of ECL-E loaded (Table 1). The PS of ECL-E at varying ratios ranged from 47.30 to 314.60 nm, as shown in Table 1. The result was similar to the study by Al-Nemrawi et al. [33], who found that CS nanoparticle sizes ranged from 145.73 to 724.23 nm. Regardless of the CS/ECL-E ratio, the smallest nanoparticles were found in those devoid of ECL-E, while the largest nanoparticles were found when CS/ECL-E at 1:1 ratio was used ($p < 0.05$). According to Hadidi et al. [22] and Hosseini et al. [34], nanoparticles became larger in size as they were loaded with the core substances. The larger diameter of ECL-E-loaded nanoparticles was mediated by the TPP-CS layer that enveloped the individual ECL-E droplets [34]. As evidenced by a high EE, in the presence of a substantial amount of ECL-E, CS might entrap more ECL-E, especially during the gelation process with the aid of ultrasonication. A smaller nanoparticle could provide the uniform entrapment or encapsulation of ECL-E. Gulzar et al. [7] noticed a similar trend in the particle diameter of CS nanoparticles loaded with shrimp oil. However, there was no difference in the particle sizes of the nanoparticles loaded with ECL-E utilizing the CS/ECL-E ratios of 1:2 and 1:3 ($p > 0.05$).

The PDI is a measure of particle size distribution in a sample. In general, the PDI ranges from 0 (monodisperse particles) to 1 (highly polydisperse particles) [35]. A lower PDI indicates a more uniform particle size distribution, which is often desirable for consistent behavior in applications [33]. ECL-E-N-E2 and ECL-E-N-E3 had the lowest PDI ($p < 0.05$) among all the nanoparticles (0.20–0.22), indicating the most homogeneity or consistency. For CS nanoparticles, a PDI value of less than 0.3 was generally considered acceptable, indicating a relatively narrow size distribution [36]. Strong repulsions among the particles may have resulted from the dispersion of positive charges on the nanoparticles' surfaces, thus reducing the coagulation or collision [23]. Consequently, ECL-E-N-E2 and ECL-E-N-E3 displayed a low PDI.

The zeta potential (ZP) of CS nanoparticles is a critical parameter in determining their stability, interaction with biological systems, and overall functionality [37,38]. ZP is the electrical potential at the slipping plane of a particle in a fluid. It indicates the degree of electrostatic repulsion or attraction between particles [38,39]. All nanoparticles carried positive charges ranging between +40.37 and +44.24 mV, which showed a similar range to the CS nanoparticles prepared by Al-Nemrawi et al. [33]. Adsorption or encapsulation of phenolic extracts in cationic carriers, such as chitosan nanoparticles, typically leads to noticeable changes in the zeta potential of these carriers. This change is primarily due to phenolic compounds, which might carry both negative charge and positively charged surface. During complex formation, the interaction between the phenolic compounds and the cationic carrier could lead to the formation of complexes or conjugates. These complexes might have a lower net positive charge or even shift the zeta potential towards

the negative value, depending on the relative amounts and the charge density of the phenolic compounds. A higher zeta potential (either positive or negative) typically reflects better stability of the nanoparticle suspension [40]. Particles with a high zeta potential repel each other and resist aggregation [41]. CS nanoparticles with a high positive zeta potential are more stable in suspension because of electrostatic repulsion [42]. CS nanoparticles often exhibit zeta potentials in the range of +30 to +60 mV, indicating good stability [43].

3.1.3. Color

The L* values of the ECL-E nanoparticles were higher ($p < 0.05$) when compared with those of free ECL-E. This could be the result of the entrapment of ECL-E in the nanoparticles, thus hiding its color [23]. In the TPP-CS encapsulation process, an increased amount of extract encapsulated resulted in a higher L* value (indicating lightness). This was because ECL-E at a higher amount was entrapped, and the surface of wall materials contributed to reflecting lighter and increasing the lightness [44]. In addition, the formation of larger particles or agglomerates could scatter light more effectively, and lighter samples could be noticed [45]. A slightly lower a* value was found in nanoparticles, compared with free ECL-E. Regarding the b* value, similar values were found between ECL-E and nanoparticles loaded with ECL-E at different CS/ECL-E ratios since ECL-E was dechlorophylized before loading into nanoparticles or encapsulation. As a result, green coloring pigments were removed, making the powder fade in color.

3.1.4. In Vitro Releasing Efficiency

Figure 1 shows the releasing efficiency (RE) of nanoparticles at different ECL-E/CS ratios in comparison to the control (1% ECL-E). The nanoparticles showed a slower release rate of ECL-E than that of the control. After 8 h of dialysis, the release profile of 1% ECL-E revealed a roughly 54% RE. RE was significantly decreased by the entrapment of ECL-E in TPP-CS gel. After 8 h, the RE of ECL-E-N-E3, ECL-E-N-E2, and ECL-E-N-E1 was 17%, 20%, and 26%, respectively. ECL-E-N-E3 exhibited the lowest release rate among all the nanoparticles after 72 h. A RE of 51% was reached for ECL-E-N-E3, followed by ECL-E-N-E2 (57%) and ECL-E-N-E1 (63%). The different ECL-E ratios acted as a mediating factor in the variation in their release rates. The reduced RE in the nanoparticle loaded with ECL-E showed that the release of ECL-E was retarded. The releasing efficiency of TPP-CS gel can be influenced by several factors. High cross-linking with TPP can lead to a slow release rate [29]. Small particles often release encapsulated compounds more quickly because of a larger surface area [46,47]. The pH sensitivity of chitosan can affect the swelling of the matrix and, consequently determine the release rate [48]. Controlled release is one of the most desired characteristics of encapsulated substances [24]. Encapsulating ECL-E into nanoparticles significantly reduced the diffusion rate, depending on the amount of ECL-E employed. Furthermore, the manufacturing method controlled their release at different rates.

3.1.5. Antioxidant Activities of TPP-CS Nanoparticles Prepared Using Different CS/ECL-E Ratios

The empty nanoparticles (without loaded ECL-E) and the nanoparticles loaded with ECL-E at varying CS/ECL-E ratios had different antioxidant activities ($p < 0.05$). The amounts of ECL-E corresponding to those entrapped in nanoparticles were used to determine antioxidant activities (Table 2). When the quantity of ECL-E entrapped in the nanoparticles was compared, a higher amount of TPC was correlated with the stronger antioxidant activity of the nanoparticles made with a higher amount of ECL-E. This result revealed that ECL-E was loaded into the nanoparticles, and the ratios affected the amount of ECL-E loaded. Table 2 shows that the produced nanoparticles could significantly increase DPPH radical scavenging, which indicated that encapsulation improved the dispersion of hydrophobic antioxidative compounds [49]. This suggested that the active ingredients in ECL-E might scavenge free radicals that were both amphiphilic (ABTS) and hydrophobic (DPPH) [23,25]. Furthermore, the FRAP assay revealed that ECL-E encapsulated in

nanoparticles might provide electrons for free radicals. Additionally, ECL-E also had metal chelating activity, indicating the binding or sequestration of metal ions, prooxidants in the process of lipid oxidation. The ORAC varied among nanoparticles made with varying ECL-E/CS ratios. The highest ORAC was found in the nanoparticles loaded with the highest ratio of ECL-E/CS. This was related to the highest EE or the active compounds loaded as the core of nanoparticles.

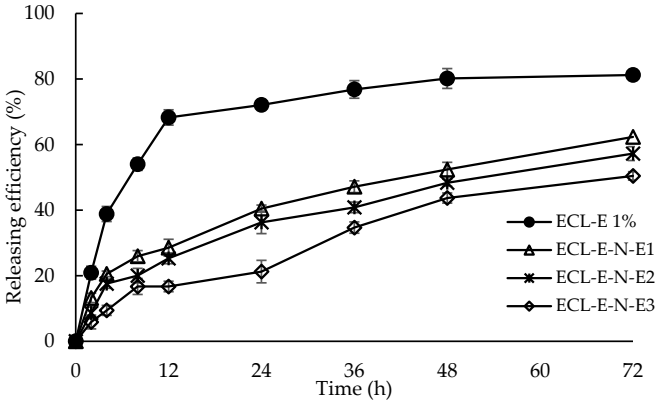

Figure 1. Release profiles of TPP-CS loaded with ECL-E at different levels in comparison with non-encapsulated ECL-E at 1% during a 72 h dialysis period at 4 °C. Bars represent standard deviations (n = 3). ECL-E-N-E1, ECL-E-N-E2, and ECL-E-N-E3 denote nanoparticles using CS/ECL-E ratios of 1:1, 1:2, and 1:3, respectively. ECL-E 1%: free extract at 1%.

Table 2. TPC and antioxidant activities of TPP-CS loaded with ECL-E at different levels in comparison with non-encapsulated ECL-E at 1%.

Treatment	TPC (mg GAE/g Dry Solid)	ABTS (μmol TE/g Dry Solid)	DPPH (mg TE/g dry Solid)	FRAP (mg TE/g Dry Solid)	MCA (μmol EE/g Dry Solid)	ORAC (μmol TE/g Dry Extract)
ECL-E	345.81 ± 16.22 ^{a}	1409.09 ± 24.26 ^{a}	362.42 ± 22.24 ^{c}	892.25 ± 36.87 ^{a}	4.51 ± 0.14 ^{c}	73.91 ± 8.67 ^{b}
TPP-CS	0.33 ± 0.07 ^{e}	2.15 ± 0.06 ^{e}	29.01 ± 0.57 ^{e}	0.08 ± 0.02 ^{e}	5.81 ± 0.41 ^{b}	120.75 ± 2.26 ^{a}
ECL-E-N-E1	47.41 ± 0.74 ^{d}	438.18 ± 0.83 ^{d}	68.81 ± 0.24 ^{d}	156.37 ± 0.35 ^{d}	6.83 ± 0.38 ^{a}	26.99 ± 1.44 ^{d}
ECL-E-N-E2	97.55 ± 0.35 ^{c}	1302.86 ± 12.06 ^{b}	1058.81 ± 1.61 ^{b}	394.20 ± 0.62 ^{c}	3.30 ± 0.31 ^{d}	28.93 ± 1.42 ^{d}
ECL-E-N-E3	253.34 ± 0.20 ^{b}	1240.80 ± 13.02 ^{c}	1112.75 ± 13.89 ^{a}	518.56 ± 0.38 ^{b}	4.73 ± 0.32 ^{c}	50.08 ± 1.31 ^{c}

CS: chitosan, TPP: sodium tripolyphosphate, ECL-E: ethanolic cashew leaf extract. Different lowercase superscripts within the same column indicate significant differences ($p < 0.05$). Mean value and SD± (n = 3).

For the TPP-CS nanoparticles or empty nanoparticles, the antioxidant activities were also evaluated, as shown in Table 2. Because the hydroxyl and amino groups in the chitosan backbone can react with free radicals, empty nanoparticles have the ability to exhibit antioxidant properties. These findings are in line with earlier research conducted by Soleymanfallah et al. [50], especially for DPPH radical scavenging activity and ORAC. For DPPH radical scavenging activity, amino (-NH_2) and hydroxyl (-OH) groups in the structure of chitosan could donate electrons or hydrogen atoms to DPPH free radicals, making DPPH free radicals stable and non-reactive [51]. At the same time, it can donate electrons or hydrogen atoms to oxygen radicals, stabilizing free radicals and reducing oxidative damage [52]. Chitosan has a high ORAC activity. Chitosan with high degree of deacetylation with more free amino groups had, the increases antioxidant capacity [53].

The nanoparticles possessed lower antioxidant activity compared with the free form. Active compounds might bind and disperse within the nanoparticle matrix, potentially lowering their immediate release into solution compared with free compounds [54–56]. When active compounds were encapsulated effectively, the amount available for antioxidant activity could be reduced [55]. A low controlled release can initially reduce the concentration of active compounds available for immediate reaction with radicals [56], which is beneficial for sustained activity.

3.1.6. Antimicrobial Activity

Different MICs and MBCs (Table 3) were found between nanoparticles loaded with ECL-E and free ECL-E ($p < 0.05$). As shown in Table 3, TPP-CS nanoparticles or empty nanoparticles showed antibacterial activity, which was attributed to chitosan's amino group ($-NH_3^+$, positive charge) binding to the bacterial cell wall (negative charge), disrupting the integrity of the cell wall and cell membrane, and possibly causing membrane damage, leakage, and cell death [57,58]. The MICs and MBCs of nanoparticles were higher than those of free ECL-E against *P. aeruginosa* and *S. putrefaciens* ($p < 0.05$), indicating that ECL-E with antimicrobial activity was entrapped within nanoparticles and the release of ECL-E was lowered. This resulted in a decrease in antibacterial activity by initially reducing the concentration of active compounds available for immediate reaction with microorganisms and delaying their antimicrobial effects [59]. Meanwhile, the active agents were also distributed throughout the nanoparticle matrix [55], in which their concentration was diluted compared with the free form. In addition, the barrier from encapsulation was an important factor, potentially limiting their immediate availability [60]. These factors could collectively contribute to decreased antimicrobial activity in nanoparticle formulations compared with free forms.

Table 3. MIC and MBC values of TPP-CS loaded with ECL-E at different levels in comparison with non-encapsulated ECL-E at 1%.

Treatment	*P. aeruginosa* (mg/mL)		*S. putrefaciens* (mg/mL)	
	MIC	**MBC**	**MIC**	**MBC**
ECL-E	2.34 ^{a}	9.38 ^{a}	1.17 ^{a}	4.69 ^{a}
TPP-CS	37.50 ^{d}	300.00 ^{d}	18.75 ^{d}	150.00 ^{c}
ECL-E-N-E1	18.75 ^{c}	150.00 ^{c}	9.38 ^{c}	75.00 ^{b}
ECL-E-N-E2	9.38 ^{b}	75.00 ^{b}	9.38 ^{c}	75.00 ^{b}
ECL-E-N-E3	9.38 ^{b}	75.00 ^{b}	4.69 ^{b}	75.00 ^{b}

CS: chitosan, TPP: sodium tripolyphosphate, ECL-E: ethanolic cashew leaf extract. Different lowercase superscripts within the same column indicate significant differences ($p < 0.05$). Mean value ($n = 3$).

3.1.7. Fourier Transform Infrared Spectroscopic Spectra

The relationship among TPP, CS, and ECL-E in the nanoparticles was verified by FTIR spectroscopy. Figure 2A shows the FTIR spectra of ECL-E and nanoparticles without and with ECL-E. The peaks at 3600–2800 cm^{-1} and 1700–400 cm^{-1} were the main peaks in the infrared spectra. This was similar to the study by Antoniou et al. [61]. The peaks at 3400–3200 cm^{-1} were a result of the −OH stretching vibration associated with free, inter-, and intramolecular bound hydroxyl groups for ECL-E [61]. In addition, these peaks might also be associated with hydroxyl groups in free chitosan and CS-TPP cross-links in nanoparticles [7]. In the same area, the peaks at ≈3300 cm^{-1} in nanoparticles were attributed to N−H (amino) group stretching [7]. Peaks in the range of 3000–2800 cm^{-1} corresponded to the typical C−H vibration [61]. The asymmetric stretching of the C−O−C bond in the glycosidic linkage appeared around 1150 cm^{-1}, while the peak at 1077 cm^{-1} corresponded to the C−O stretching vibration [61]. The peaks in the range of 1220–1080 cm^{-1} were attributed to P=O stretching, while the absorption bands at 843 cm^{-1} corresponded to P−O and P−O−P in the TPP spectrum [61]. Additionally, the peak at 1204 cm^{-1} in the nanoparticle spectra indicated P=O stretching, resulting from the cross-linking between CS and TPP [62]. The bioactive chemicals in ECL-E exhibited strong peaks at the following wavenumbers: 3383 cm^{-1}, which corresponded to O–H stretching; 1544 cm^{-1}, which represented C=C stretching; 1447 cm^{-1}, which corresponded to C–C stretching; and 1037 cm^{-1}, which indicated C–O–C stretching (Figure 2) [63]. A portion of these peaks were found in ECL-E-Ns. Finally, the peak for N−H bending vibration of primary amines at 1639 cm^{-1} in the nanoparticle spectra shifted to 1626 cm^{-1} when loaded with ECL-E in ECL-E-Ns. These results indicated the interaction between ECL-E and nanoparticles. The emergence

of these peaks signifies the production of nanoparticles and the enhancement of inter- and intramolecular interactions in nanoparticles.

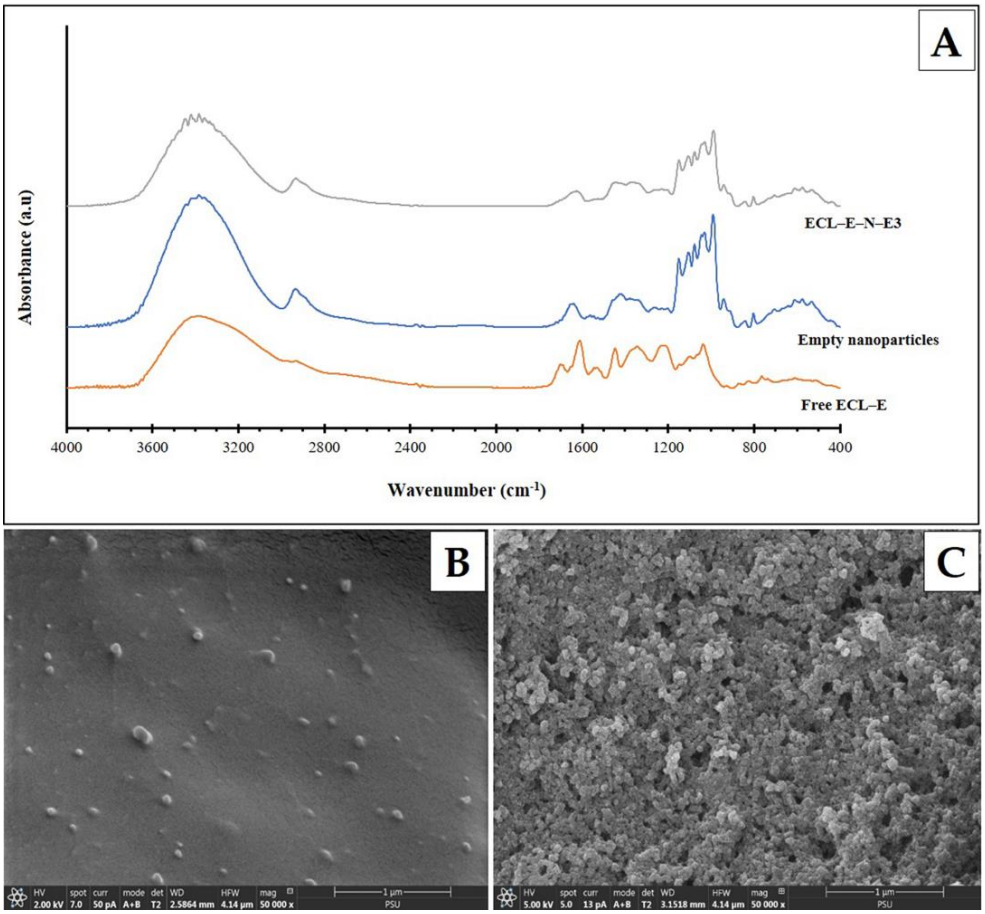

Figure 2. FTIR spectra of free ECL-E, empty nanoparticles, and ECL-E-N-E3 (**A**). Scanning electron micrographs of empty nanoparticles (**B**) and ECL-E-N-E3 (**C**). ECL-E-N-E3: nanoparticles using CS/ECL-E ratios of 1:3; Free ECL-E: free extract at 1%.

3.1.8. Scanning Electron Microscopic Images

The nanoparticles were spherical and nanometer in size, as displayed in Figure 2B,C. In Figure 2C, the nanoparticles loaded with ECL-E have a continuous and regular shape. Their morphology could be affected by the freeze-drying method. During drying, particles align closer together and bind together [64,65]. Figure 2B represents nanoparticles without ECL-E loaded, which had an uneven distribution because of the fact that the nanoparticles without ECL-E loaded did not have the core of the extract [65,66]. The particle size was thus smaller than nanoparticles loaded with ECL-E, as shown in Table 1. Figure 2C shows that the nanoparticles loaded with ECL-E have larger particle diameters (Table 1). The nanoparticles in each treatment had varying particle sizes. Size could be governed by the electrostatic interaction of TPP and CS in the ionic gelation process and was dependent on the mixing occurring during preparation [7].

3.2. Light Stability of TPP-CS Nanoparticles Loaded with ECL-E as Affected by Light at Various Intensities

Figure 3 illustrates the TPC, ABTS, and DPPH radical scavenging activities and FRAP of nanoparticles loaded with ECL-E. The TPC and antioxidant activities of nanoparticles exposed to light increased in the first 48 h and then progressively declined after 72 h. The increased light intensity caused the rapid degradation, in which some products with antioxidant properties were produced. Esua et al. [67] also found a similar result, in which

the antioxidant of tomato dried for a longer time had increased antioxidant activity. As shown in Figure 3, the period of exposure was another significant factor that influenced the breakdown of phenolic compounds. For the longest duration (144 h), the nanoparticles were exposed to the maximum intensity of light (4000 lux). This resulted in the greatest losses in TPC and, naturally antioxidant activities.

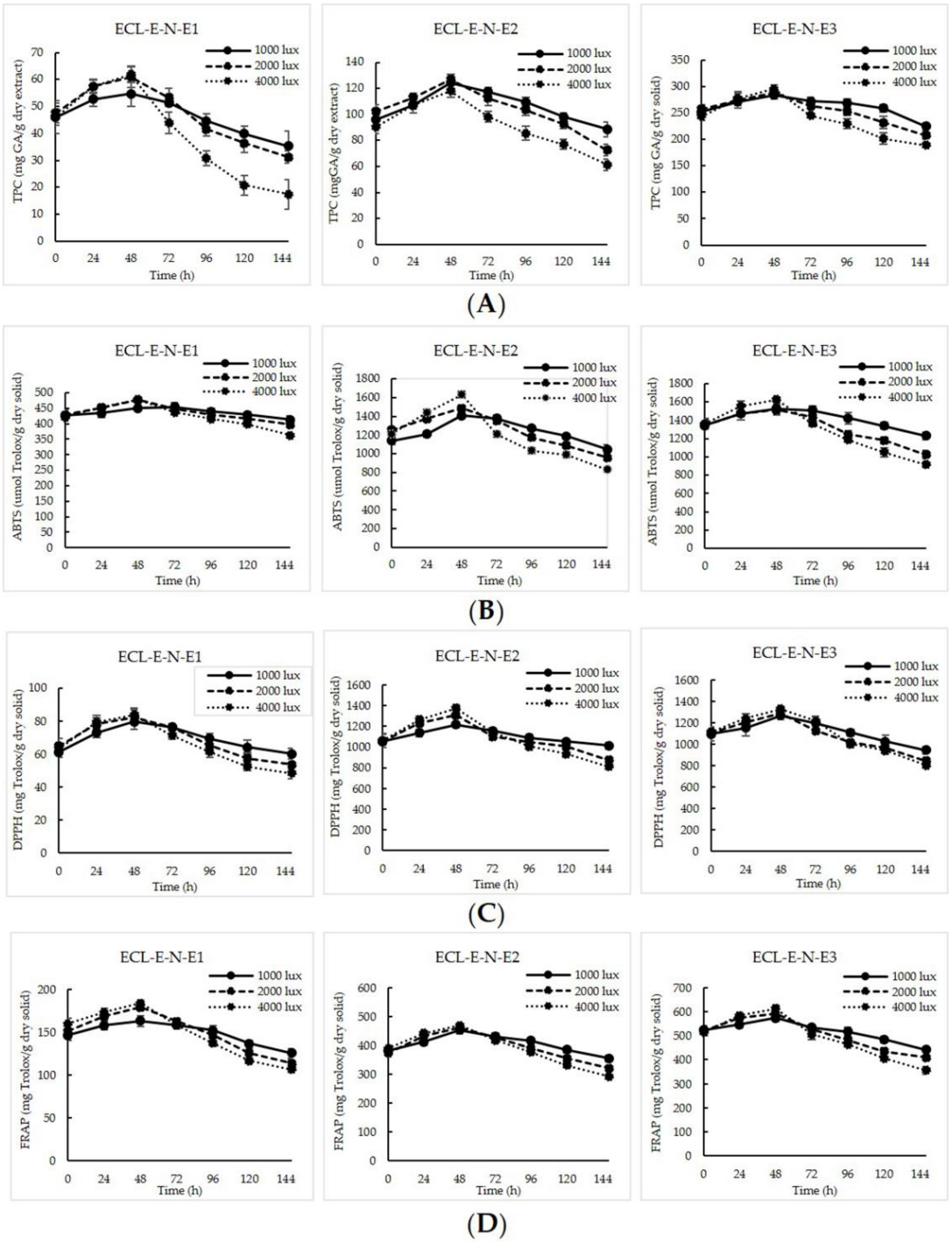

Figure 3. Effect of light at different intensities and times on the total phenolic content (TPC, (**A**)), ABTS radical scavenging activity (ABTS, (**B**)), DPPH radical scavenging activity (DPPH, (**C**)), and ferric reducing antioxidant power (FRAP, (**D**)) of TPP-CS loaded with ECL-E at different levels. Bars represent standard deviations (n = 3). ECL-E-N-E1, ECL-E-N-E2, and ECL-E-N-E3 denote nanoparticles using CS/ECL-E ratios of 1:1, 1:2, and 1:3, respectively.

Light intensity can affect nanoparticles by causing degradation or structural changes, especially UV, which can degrade chitosan, breaking down its molecular structure [12,68,69]. At the same time, high-intensity light can increase the temperature, potentially affecting the stability of the nanoparticles [70]. These effects can reduce the effectiveness and stability of chitosan nanoparticles. This was evidenced by an increase in TPC and antioxidant activities. Because of the damage to nanoparticles, the ECL-E inside was released. When the ECL-E was released freely, polyphenols with several OH groups could possess a high capacity as antioxidants. However, those compounds were mostly light-sensitive [71]. Therefore, it decomposes and loses its antioxidant activities easily. Nevertheless, those compounds could be protected or the loss of bioactive compounds in ECL-E could be delayed to a certain extent when compared with free ECL-E (un-encapsulation) [3]. This result was also in accordance with the study on cashew leaf extract by Sinlapapanya et al. [3], who documented that TPC decreased when exposed to light and decreased to a higher extent when exposed to high-intensity light.

4. Conclusions

Encapsulation of ECL-E with TPP-CS nanoparticles by the ionic gelation method was carried out. The ECL-E-N-E3 nanoparticles exhibited excellent physical properties and bioactivities. It had a pale color, tiny particle size, positive zeta potential, and low PDI with high antioxidant and antibacterial activities. The ECL-E/CS ratio had a significant impact on the interaction among TPP, CS, and ECL-E for the creation of nanoparticles. Furthermore, it also affected the shape of nanoparticles. The nanoparticles demonstrated a protective effect against the loss of ECL-E activity induced by light intensity and also played a significant function in regulating the rate of ECL-E release. Thus, ECL-E encapsulated with TPP-CS nanoparticles could serve as a delivery vehicle with enhanced stability by maintaining the antioxidant activity and antibacterial activity of ECL-E.

Author Contributions: Conceptualization, P.S., J.B. and S.B.; methodology, P.S. and J.B.; validation, P.S., J.B. and S.B.; formal analysis, P.S.; investigation, P.S. and S.B.; resources, S.B.; data curation, P.S.; writing—original draft preparation, P.S.; writing—review and editing, S.P., R.A.N., B.Z., T.P. and S.B.; supervision, S.B.; project administration, S.B.; funding acquisition, S.B. All authors have read and agreed to the published version of the manuscript.

Funding: This study was funded by a Prachayacharn grant from Prince of Songkla University (Grant No. AGR6602079N) and the National Research Council of Thailand (NRCT) under the International Research Network (IRN) program.

Data Availability Statement: The original contributions presented in the study are included in the article, further inquiries can be directed to the corresponding author.

Acknowledgments: The authors would like to thank the International Center of Excellence in Seafood Science and Innovation, Faculty of Agro-Industry, Prince of Songkla University for the facilities provided for all the experiments.

Conflicts of Interest: The authors declare no conflicts of interest.

References

1. Pinto, T.; Aires, A.; Cosme, F.; Bacelar, E.; Morais, M.C.; Oliveira, I.; Ferreira-Cardoso, J.; Anjos, R.; Vilela, A.; Gonçalves, B. Bioactive (poly) Phenols, Volatile Compounds from Vegetables, Medicinal and Aromatic Plants. *Foods* **2021**, *10*, 106. [CrossRef] [PubMed]
2. Sinlapapanya, P.; Sumpavapol, P.; Nirmal, N.; Zhang, B.; Hong, H.; Benjakul, S. Ethanolic Cashew Leaf Extract: Antimicrobial Activity, Mode of Action, and Retardation of Spoilage Bacteria in Refrigerated Nile Tilapia Slices. *Foods* **2022**, *11*, 3461. [CrossRef]
3. Sinlapapanya, P.; Sumpavapol, P.; Buatong, J.; Benjakul, S. Ethanolic Cashew Leaf Extract: Antioxidant Potential and Impact on Quality Changes of Dried Fermented Catfish During Storage. *Future Foods* **2024**, *9*, 100296. [CrossRef]
4. Cao, H.; Saroglu, O.; Karadag, A.; Diaconeasa, Z.; Zoccatelli, G.; Conte-Junior, C.A.; Gonzalez-Aguilar, G.A.; Ou, J.; Bai, W.; Zamarioli, C.M.; et al. Available Technologies on Improving The Stability of Polyphenols in Food Processing. *Food Front.* **2021**, *2*, 109–139. [CrossRef]

5. Yin, Z.; Zheng, T.; Ho, C.T.; Huang, Q.; Wu, Q.; Zhang, M. Improving The Stability and Bioavailability of Tea Polyphenols by Encapsulations: A review. *Food Sci. Hum. Wellness* **2022**, *11*, 537–556. [CrossRef]
6. Assadpour, E.; Jafari, S.M. Advances in Spray-Drying Encapsulation of Food Bioactive Ingredients: From Microcapsules to Nanocapsules. *Annu. Rev. Food Sci. Technol.* **2019**, *10*, 103–131. [CrossRef]
7. Gulzar, S.; Raju, N.; Prodpran, T.; Benjakul, S. Chitosan-Tripolyphosphate Nanoparticles Improves Oxidative Stability of Encapsulated Shrimp Oil Throughout The Extended Storage. *Eur. J. Lipid Sci. Technol.* **2022**, *124*, 2100178. [CrossRef]
8. Maleki, G.; Woltering, E.J.; Mozafari, M.R. Applications of Chitosan-Based Carrier as an Encapsulating Agent in Food Industry. *Trends Food Sci. Technol.* **2022**, *120*, 88–99. [CrossRef]
9. Akhavan, S.; Assadpour, E.; Katouzian, I.; Jafari, S.M. Lipid Nano Scale Cargos for The Protection and Delivery of Food Bioactive Ingredients and Nutraceuticals. *Trends Food Sci. Technol.* **2018**, *74*, 132–146. [CrossRef]
10. Rostami, M.; Yousefi, M.; Khezerlou, A.; Mohammadi, M.A.; Jafari, S.M. Application of Different Biopolymers for Nanoencapsulation of Antioxidants via Electrohydrodynamic Processes. *Food Hydrocoll.* **2019**, *97*, 105170. [CrossRef]
11. Jacob, P.L.; Brugnoli, B.; Del Giudice, A.; Phan, H.; Chauhan, V.M.; Beckett, L.; Gillis, R.B.; Moloney, C.; Cavanagh, R.J.; Krumins, E.; et al. Poly (diglycerol adipate) Variants as Enhanced Nanocarrier Replacements in Drug Delivery Applications. *J. Colloid Interface Sci.* **2023**, *641*, 1043–1057. [CrossRef] [PubMed]
12. Wang, W.; Xue, C.; Mao, X. Chitosan: Structural Modification, Biological Activity and Application. *Int. J. Biol. Macromol.* **2020**, *164*, 4532–4546. [CrossRef] [PubMed]
13. Seidi, F.; Yazdi, M.K.; Jouyandeh, M.; Dominic, M.; Naeim, H.; Nezhad, M.N.; Bagheri, B.; Habibzadeh, S.; Zarrintaj, P.; Saeb, M.R.; et al. Chitosan-Based Blends for Biomedical Applications. *Int. J. Biol. Macromol.* **2021**, *183*, 1818–1850. [CrossRef] [PubMed]
14. Kumari, S.; Kishor, R. Chapter 1-Chitin and Chitosan: Origin, Properties, and Applications. In *Handbook of Chitin and Chitosan*; Gopi, S., Thomas, S., Pius, A., Eds.; Elsevier: Amsterdam, The Netherlands, 2020; pp. 1–33.
15. Pellis, A.; Guebitz, G.M.; Nyanhongo, G.S. Chitosan: Sources, Processing and Modification Techniques. *Gels* **2022**, *8*, 393. [CrossRef] [PubMed]
16. Brugnoli, B.; Mariano, A.; Simonis, B.; Bombelli, C.; Sennato, S.; Piozzi, A.; Taresco, V.; Chauhan, V.M.; Howdle, S.M.; d'Abusco, A.S.; et al. Self-assembled Chitosan-sodium Caseinate Drug Delivery Nanosystems: Synthesis, Characterization, Stability Studies, in vitro Cytotoxicity and in vivo Biocompatibility against 143 B Cells. *Carbohydr. Polym. Technol. Appl.* **2023**, *6*, 100373. [CrossRef]
17. Shafiei, M.; Jafarizadeh-Malmiri, H.; Rezaei, M. Biological Activities of Chitosan and Prepared Chitosan-Tripolyphosphate Nanoparticles using Ionic Gelation Method Against Various Pathogenic Bacteria and Fungi Strains. *Biologia* **2019**, *74*, 1561–1568. [CrossRef]
18. Gutiérrez-Ruíz, S.C.; Cortes, H.; González-Torres, M.; Almarhoon, Z.M.; Gürer, E.S.; Sharifi-Rad, J.; Leyva-Gómez, G. Optimize The Parameters for The Synthesis By The Ionic Gelation Technique, Purification, and Freeze-Drying of Chitosan-Sodium Tripolyphosphate Nanoparticles for Biomedical Purposes. *J. Biol. Eng.* **2024**, *18*, 12. [CrossRef]
19. Akbari-Alavijeh, S.; Shaddel, R.; Jafari, S.M. Encapsulation of Food Bioactives and Nutraceuticals By Various Chitosan-Based Nanocarriers. *Food Hydrocoll.* **2020**, *105*, 105774. [CrossRef]
20. Di Santo, M.C.; D'Antoni, C.L.; Rubio, A.P.D.; Alaimo, A.; Pérez, O.E. Chitosan-Tripolyphosphate Nanoparticles Designed to Encapsulate Polyphenolic Compounds for Biomedical and Pharmaceutical Applications—A review. *Biomed. Pharmacother.* **2021**, *142*, 111970. [CrossRef] [PubMed]
21. Shetta, A.; Kegere, J.; Mamdouh, W. Comparative Study of Encapsulated Peppermint and Green Tea Essential Oils in Chitosan Nanoparticles: Encapsulation, Thermal Stability, In-vitro Release, Antioxidant and Antibacterial Activities. *Int. J. Biol. Macromol.* **2019**, *126*, 731–742. [CrossRef] [PubMed]
22. Hadidi, M.; Pouramin, S.; Adinepour, F.; Haghani, S.; Jafari, S.M. Chitosan Nanoparticles Loaded with Clove Essential Oil: Characterization, Antioxidant and Antibacterial Activities. *Carbohydr. Polym.* **2020**, *236*, 116075. [CrossRef] [PubMed]
23. Tagrida, M.; Prodpran, T.; Zhang, B.; Aluko, R.E.; Benjakul, S. Liposomes Loaded with Betel Leaf (*Piper betle* L.) Ethanolic Extract Prepared by Thin Film Hydration and Ethanol Injection Methods: Characteristics and Antioxidant Activities. *J. Food Biochem.* **2021**, *45*, e14012. [CrossRef] [PubMed]
24. Olatunde, O.O.; Benjakul, S.; Vongkamjan, K.; Amnuaikit, T. Liposomal Encapsulated Ethanolic Coconut Husk Extract: AntiOxidant and Antibacterial Properties. *J. Food Sci.* **2019**, *84*, 3664–3673. [CrossRef] [PubMed]
25. Benjakul, S.; Kittiphattanabawon, P.; Sumpavapol, P.; Maqsood, S. Antioxidant Activities of Lead (*Leucaena leucocephala*) Seed as Affected By Extraction Solvent, Prior Dechlorophyllisation and Drying Methods. *J. Food Sci. Technol.* **2014**, *51*, 3026–3037. [CrossRef]
26. Sae-Leaw, T.; O'Callaghan, Y.C.; Benjakul, S.; O'Brien, N.M. Antioxidant Activities and Selected Characteristics of Gelatin Hydrolysates from Seabass (*Lates calcarifer*) Skin as Affected by Production Processes. *J. Food Sci. Technol.* **2016**, *53*, 197–208. [CrossRef] [PubMed]
27. Lopez, M.K.N.; Hadisurya, M.; Cornwall, R.G. Antimicrobial Investigation and Structure Activity Analysis of Natural Eugenol Derivatives Against Several Oral Bacteria. *J. Pharm. Microbiol.* **2019**, *5*, 1–4.
28. Jafarı-sales, A.; Jafari, B.; Khaneshpour, H.; Pashazadeh, M. Antibacterial Effect of Methanolic Extract of Rosa Damascena on Standard Bacteria *Staphylococcus aureus*, *Bacillus cereus*, *Escherichia coli* and *Pseudomonas aeruginosa* In Vitro. *Int. J. Nat. Life Sci.* **2020**, *4*, 40–46.

29. Kadam, D.; Lele, S.S. Cross-Linking Effect of Polyphenolic Extracts of *Lepidium sativum* Seedcake on Physicochemical Properties of Chitosan Films. *Int. J. Biol. Macromol.* **2018**, *114*, 1240–1247. [CrossRef]
30. Wahba, M.I. Enhancement of The Mechanical Properties of Chitosan. *J. Biomater. Sci. Polym. Ed.* **2020**, *31*, 350–375. [CrossRef]
31. Da Rosa, C.G.; Borges, C.D.; Zambiazi, R.C.; Rutz, J.K.; da Luz, S.R.; Krumreich, F.D.; Benvenutti, E.V.; Nunes, M.R. Encapsulation of The Phenolic Compounds of The Blackberry (*Rubus fruticosus*). *LWT-Food Sci. Technol.* **2014**, *58*, 527–533. [CrossRef]
32. Kaushalya, K.G.D.; Gunathilake, K.D.P.P. Encapsulation of Phlorotannins From Edible Brown Seaweed in Chitosan: Effect of Fortification on Bioactivity and Stability in Functional Foods. *Food Chem.* **2022**, *377*, 132012. [CrossRef] [PubMed]
33. Al-Nemrawi, N.K.; Alsharif, S.S.M.; Dave, R.H. Preparation of Chitosan-TPP Nanoparticles: The Influence of Chitosan Polymeric Properties and Formulation Variables. *Int. J. Appl. Pharm.* **2018**, *10*, 60–65. [CrossRef]
34. Hosseini, S.F.; Zandi, M.; Rezaei, M.; Farahmandghavi, F. Two-Step Method for Encapsulation of Oregano Essential Oil in Chitosan Nanoparticles: Preparation, Characterization and In Vitro Release Study. *Carbohydr. Polym.* **2013**, *95*, 50–56. [CrossRef]
35. Danaei, M.R.M.M.; Dehghankhold, M.; Ataei, S.; Hasanzadeh Davarani, F.; Javanmard, R.; Dokhani, A.; Khorasani, S.; Mozafari, M.R. Impact of Particle Size and Polydispersity Index on The Clinical Applications of Lipidic Nanocarrier Systems. *Pharmaceutics* **2018**, *10*, 57. [CrossRef] [PubMed]
36. Yan, Q.; Weng, J.; Wu, X.; Wang, W.; Yang, Q.; Guo, F.; Wu, D.; Song, Y.; Chen, F.; Yang, G. Characteristics, Cryoprotection Evaluation and In Vitro Release of BSA-Loaded Chitosan Nanoparticles. *Mar. Drugs* **2020**, *18*, 315. [CrossRef]
37. Ferreira, L.M.; Dos Santos, A.M.; Boni, F.I.; Dos Santos, K.C.; Robusti, L.M.G.; de Souza, M.P.; Ferreira, N.N.; Carvalho, S.G.; Cardoso, V.M.O.; Chorilli, M.; et al. Design of Chitosan-Lased Particle Systems: A Review of The Physicochemical Foundations for Tailored Properties. *Carbohydr. Polym.* **2020**, *250*, 116968. [CrossRef]
38. Cano-Sarmiento, C.T.D.I.; Téllez-Medina, D.I.; Viveros-Contreras, R.; Cornejo-Mazón, M.; Figueroa-Hernández, C.Y.; García-Armenta, E.; Alamilla-Beltrán, L.; García, H.S.; Gutiérrez-López, G.F. Zeta Potential of Food Matrices. *Food Eng. Rev.* **2018**, *10*, 113–138. [CrossRef]
39. Prakash, S.; Mishra, R.; Malviya, R.; Sharma, P.K. Measurement Techniques and Pharmaceutical Applications of Zeta Potential: A Review. *J. Chronother. Drug Deliv.* **2014**, *5*, 33–40.
40. Cacua, K.; Ordoñez, F.; Zapata, C.; Herrera, B.; Pabón, E.; Buitrago-Sierra, R. Surfactant Concentration and pH Effects on The Zeta Potential Values of Alumina Nanofluids to Inspect Stability. *Colloids Surf. A Physicochem. Eng. Asp.* **2019**, *583*, 123960. [CrossRef]
41. Shrestha, S.; Wang, B.; Dutta, P. Nanoparticle Processing: Understanding and Controlling Aggregation. *Adv. Colloid Interface Sci.* **2020**, *279*, 102162. [CrossRef] [PubMed]
42. Collado-González, M.; Montalbán, M.G.; Peña-García, J.; Pérez-Sánchez, H.; Víllora, G.; Baños, F.G.D. Chitosan as Stabilizing Agent for Negatively Charged Nanoparticles. *Carbohydr. Polym.* **2017**, *161*, 63–70. [CrossRef]
43. Ozturk, K.; Arslan, F.B.; Tavukcuoglu, E.; Esendagli, G.; Calis, S. Aggregation of Chitosan Nanoparticles in Cell Culture: Reasons and Resolutions. *Int. J. Pharm.* **2020**, *578*, 119119. [CrossRef] [PubMed]
44. Haas, K.; Obernberger, J.; Zehetner, E.; Kiesslich, A.; Volkert, M.; Jaeger, H. Impact of Powder Particle Structure on The Oxidation Stability and Color of Encapsulated Crystalline and Emulsified Carotenoids in Carrot Concentrate Powders. *J. Food Eng.* **2019**, *263*, 398–408. [CrossRef]
45. Zubko, E.; Shkuratov, Y.; Videen, G. Effect of Morphology on Light Scattering By Agglomerates. *J. Quant. Spectrosc. Radiat. Transf.* **2015**, *150*, 42–54. [CrossRef]
46. Saifullah, M.; Shishir, M.R.I.; Ferdowsi, R.; Rahman, M.R.T.; Van Vuong, Q. Micro and Nano Encapsulation, Retention and Controlled Release of Flavor and Aroma Compounds: A Critical Review. *Trends Food Sci. Technol.* **2019**, *86*, 230–251. [CrossRef]
47. Jafari, S.M.; He, Y.; Bhandari, B. Role of Powder Particle Size on The Encapsulation Efficiency of Oils During Spray Drying. *Dry. Technol.* **2007**, *25*, 1081–1089. [CrossRef]
48. Rizwan, M.; Yahya, R.; Hassan, A.; Yar, M.; Azzahari, A.D.; Selvanathan, V.; Sonsudin, F.; Abouloula, C.N. pH Sensitive Hydrogels in Drug Delivery: Brief History, Properties, Swelling, and Release Mechanism, Material Selection and Applications. *Polymers* **2017**, *9*, 137. [CrossRef] [PubMed]
49. Shah, B.R.; Zhang, C.; Li, Y.; Li, B. Bioaccessibility and Antioxidant Activity of Curcumin after Encapsulated by Nano and Pickerng Emulsion Based on Chitosan-Tripolyphosphate Nanoparticles. *Food Res. Int.* **2016**, *89*, 399–407. [CrossRef]
50. Soleymanfallah, S.; Khoshkhoo, Z.; Hosseini, S.E.; Azizi, M.H. Preparation, Physical Properties, and Evaluation of Antioxidant Capacity of Aqueous Grape Extract Loaded in Chitosan-TPP Nanoparticles. *Food Sci. Nutr.* **2022**, *10*, 3272–3281. [CrossRef]
51. Abd El-Hack, M.E.; El-Saadony, M.T.; Shafi, M.E.; Zabermawi, N.M.; Arif, M.; Batiha, G.E.; Khafaga, A.F.; El-Hakim, Y.M.A.; Al-Sagheer, A.A. Antimicrobial and Antioxidant Properties of Chitosan and Its Derivatives and Their Applications: A Review. *Int. J. Biol. Macromol.* **2020**, *164*, 2726–2744. [CrossRef]
52. Li, Q.; Mi, Y.; Tan, W.; Guo, Z. Highly Efficient Free Radical-Scavenging Property of Phenolic-Functionalized Chitosan Derivatives: Chemical Modification and Activity Assessment. *Int. J. Biol. Macromol.* **2020**, *164*, 4279–4288. [CrossRef] [PubMed]
53. Hao, W.; Li, K.; Ma, Y.; Li, R.; Xing, R.; Yu, H.; Li, P. Preparation and Antioxidant Activity of Chitosan Dimers with Different Sequences. *Mar. Drugs* **2021**, *19*, 366. [CrossRef] [PubMed]
54. Ge, X.; Cao, Z.; Chu, L. The Antioxidant Effect of The Metal and Metal-Oxide Nanoparticles. *Antioxidants* **2022**, *11*, 791. [CrossRef] [PubMed]
55. Maqsoudlou, A.; Assadpour, E.; Mohebodini, H.; Jafari, S.M. The Influence of Nanodelivery Systems on the Antioxidant Activity of Natural Bioactive Compounds. *Crit. Rev. Food Sci. Nutr.* **2022**, *62*, 3208–3231. [CrossRef]

56. Li, Q.; Duan, M.; Liu, L.; Chen, X.; Fu, Y.; Li, J.; Zhao, T.; McClements, D.J. Impact of Polyphenol Interactions with Titanium dioxide Nanoparticles on Their Bioavailability and Antioxidant Activity. *J. Agric. Food Chem.* **2021**, *69*, 9661–9670. [CrossRef]
57. Yilmaz Atay, H. Antibacterial Activity of Chitosan-Based Systems. In *Functional Chitosan: Drug Delivery and Biomedical Applications*; Jana, S., Jana, S., Eds.; Springer: Singapore, 2019; pp. 457–489.
58. Koilparambil, D.; Varghese, S.; Shaikmoideen, J.M. Chitosan Nanoparticles: A Novel Antimicrobial Agent. In *Nanobiotechnology in Diagnosis, Drug Delivery, and Treatment*; Rai, M., Razzaghi-Abyaneh, M., Ingle, A.P., Eds.; John Wiley and Sons: Chichester, UK, 2020; pp. 197–215.
59. Kuai, L.; Liu, F.; Chiou, B.S.; Avena-Bustillos, R.J.; McHugh, T.H.; Zhong, F. Controlled Release of Antioxidants from Active Food Packaging: A Review. *Food Hydrocoll.* **2021**, *120*, 106992. [CrossRef]
60. Subroto, E.; Andoyo, R.; Indiarto, R. Solid Lipid Nanoparticles: Review of The Current Research on Encapsulation and Delivery Systems for Active and Antioxidant Compounds. *Antioxidants* **2023**, *12*, 633. [CrossRef]
61. Antoniou, J.; Liu, F.; Majeed, H.; Qi, J.; Yokoyama, W.; Zhong, F. Physicochemical and Morphological Properties of Size-Controlled Chitosan–Tripolyphosphate Nanoparticles. *Colloids Surf. A Physicochem. Eng. Asp.* **2015**, *465*, 137–146. [CrossRef]
62. Khoerunnisa, F.; Nurhayati, M.; Dara, F.; Rizki, R.; Nasir, M.; Aziz, H.A.; Hendrawan, H.; Poh, N.E.; Kaewsaneha, C.; Opaprakasit, P. Physicochemical Properties of TPP-Crosslinked Chitosan Nanoparticles as Potential Antibacterial Agents. *Fibers Polym.* **2021**, *22*, 2954–2964. [CrossRef]
63. Lubis, L.D.; Prananda, A.T.; Juwita, N.A.; Nasution, M.A.; Syahputra, R.A.; Sumaiyah, S.; Lubis, R.R.; Lubis, M.F.; Astyka, R.; Atiqah, J.F. Unveiling Antioxidant Capacity of Standardized Chitosan-Tripolyphosphate Microcapsules Containing PolyPhenol-Rich Extract of *Portulaca oleraceae*. *Heliyon* **2024**, *10*, e29541. [CrossRef]
64. Luo, W.C.; Beringhs, A.O.R.; Kim, R.; Zhang, W.; Patel, S.M.; Bogner, R.H.; Lu, X. Impact of Formulation on The Quality and Stability of Freeze-Dried Nanoparticles. *Eur. J. Pharm. Biopharm.* **2021**, *169*, 256–267. [CrossRef] [PubMed]
65. Tchabo, W.; Ma, Y.; Kaptso, G.K.; Kwaw, E.; Cheno, R.W.; Wu, M.; Osae, R.; Ma, S.; Farooq, M. Carrier Effects on The Chemical and Physical Properties of Freeze-Dried Encapsulated Mulberry Leaf Extract Powder. *Acta Chim. Slov.* **2018**, *65*, 823–835. [CrossRef] [PubMed]
66. Wais, U.; Jackson, A.W.; He, T.; Zhang, H. Nanoformulation and Encapsulation Approaches for Poorly Water-Soluble Drug Nanoparticles. *Nanoscale* **2016**, *8*, 1746–1769. [CrossRef] [PubMed]
67. Esua, O.J.; Chin, N.L.; Yusof, Y.A.; Sukor, R. Effects of Simultaneous UV-C Radiation and Ultrasonic Energy Postharvest Treatment on Bioactive Compounds and Antioxidant Activity of Tomatoes During Storage. *Food Chem.* **2019**, *270*, 113–122. [CrossRef]
68. Yue, W.; Yao, P.; Wei, Y.; Mo, H. Synergetic Effect of Ozone and Ultrasonic Radiation on Degradation of Chitosan. *Polym. Degrad. Stab.* **2008**, *93*, 1814–1821. [CrossRef]
69. Bussiere, P.O.; Gardette, J.L.; Rapp, G.; Masson, C.; Therias, S. New Insights into The Mechanism of Photodegradation of Chitosan. *Carbohydr. Polym.* **2021**, *259*, 117715. [CrossRef]
70. Harish, V.; Ansari, M.M.; Tewari, D.; Yadav, A.B.; Sharma, N.; Bawarig, S.; García-Betancourt, M.L.; Karatutlu, A.; Bechelany, M.; Barhoum, A. Cutting-Edge Advances in Tailoring Size, Shape, and Functionality of Nanoparticles and Nanostructures: A review. *J. Taiwan Inst. Chem. Eng.* **2023**, *149*, 105010. [CrossRef]
71. Esparza, I.; Cimminelli, M.J.; Moler, J.A.; Jiménez-Moreno, N.; Ancín-Azpilicueta, C. Stability of Phenolic Compounds in Grape Stem Extracts. *Antioxidants* **2020**, *9*, 720. [CrossRef]